Cell Reports, Volume *36*

Supplemental information

Negative charge in the RACK1 loop broadens the translational capacity of the human ribosome

Madeline G. Rollins, Manidip Shasmal, Nathan Meade, Helen Astar, Peter S. Shen, and Derek Walsh

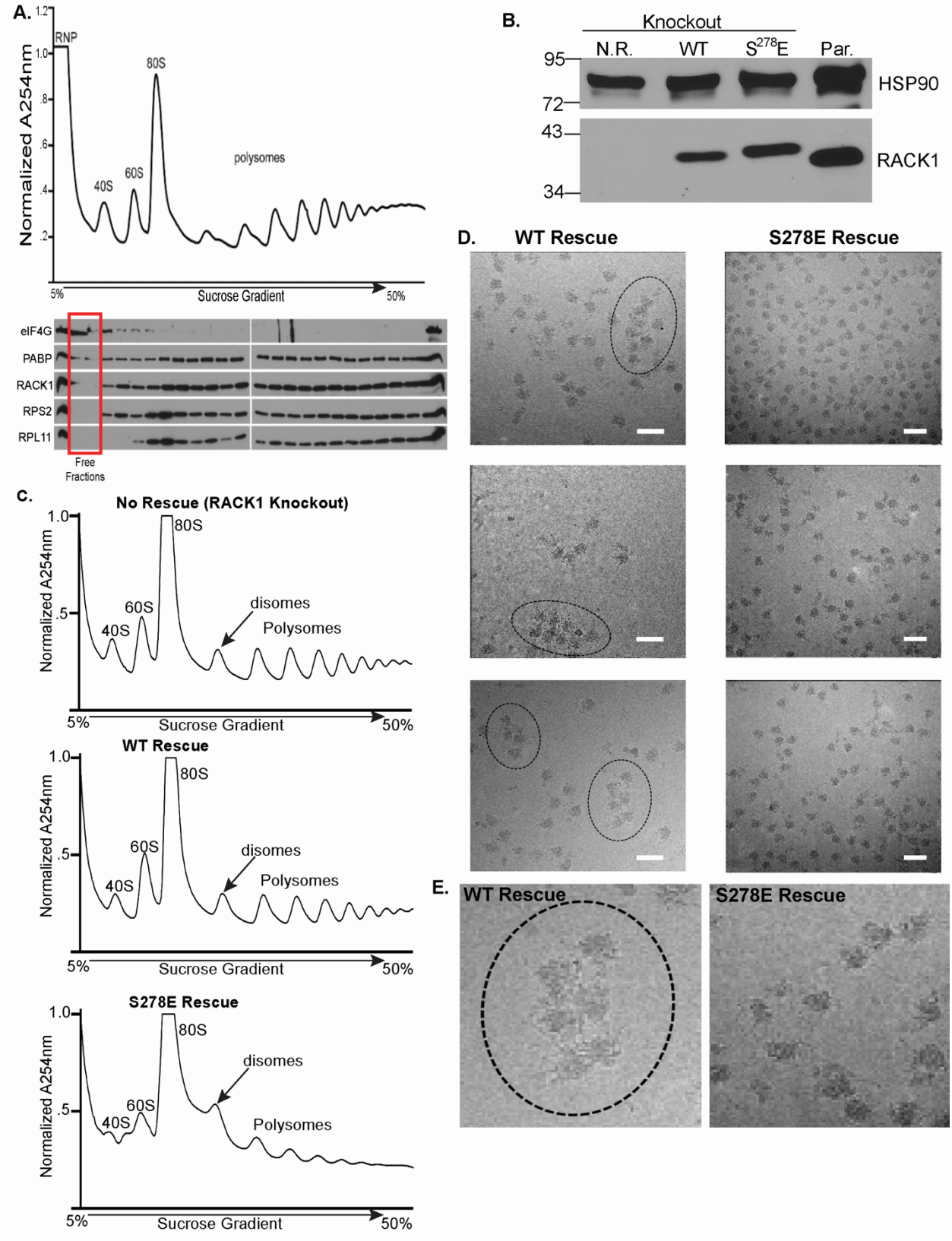

Figure S1: Characterization of a RACK1 rescue system in HAP1 cells, related to Figure 1. (A) Absorbance traces and Western blot analysis of free, 40S, 60S, 80S and polysome fractions from parental HAP1 cells. L = Lysate. Free or extra-ribosomal fractions are indicated by the red box; initiation factor eIF4G is readily detected in

both free and initiating 40S/80S fractions. RNA binding proteins such as PABP are detectable in all fractions, while RPs including RACK1 are restricted to ribosomal fractions. (B) Western blot analysis showing the relative expression of RACK1 in parental (Par.) HAP1 cells from A. compared with no rescue (N.R.) RACK1 knockouts that were rescued with either WT or $S^{278}E$ forms of RACK1. (C) Labeling highlights 40S and 60S subunits, 80S monosomes, disomes and polysomes in RACK1 knockout cells that were either not rescued or were rescued with WT or $S^{278}E$ forms of RACK1. There is a notable reduction in polysomes and an increase in monosomes and disomes specifically in cells expressing $S^{278}E$ RACK1. (D-E) Cryo-EM micrographs of ribosomes isolated by anti-Flag rapid purification from cells expressing Flag-tagged WT or $S^{278}E$ RACK1. Scale bars = 50 nm. Zoom shown in E. highlights polysomes readily observed in WT RACK1 samples, and monosome and disomes that are prevalent in $S^{278}E$ samples.

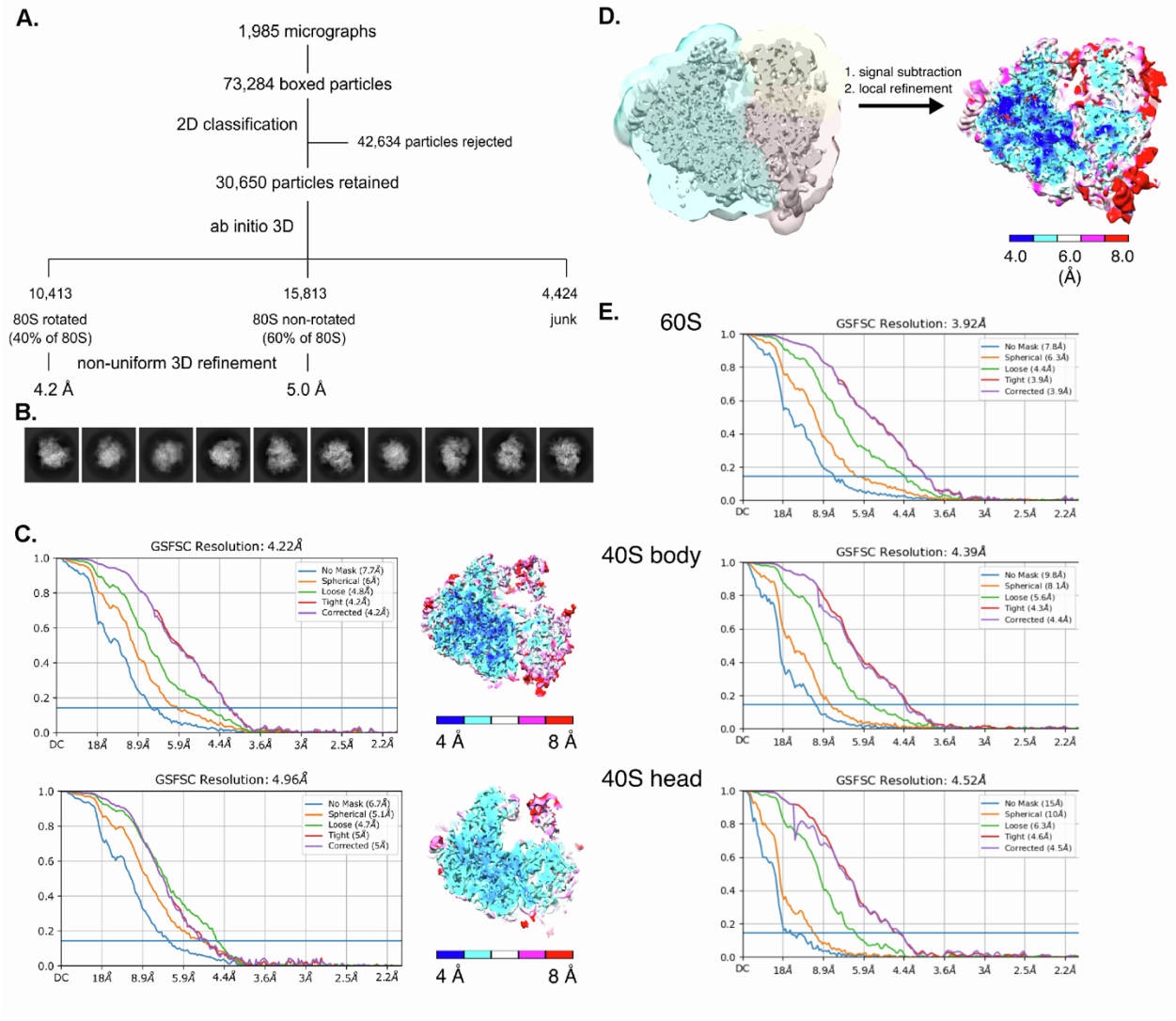

Figure S2. WT RACK1 cryo-EM data processing pipeline and local refinement of the 80S rotated state, related to Figure 1 and 5. (A) Data processing workflow and 3D classification scheme. (B) Representative reference-free 2D class averages of retained particles. (C) Gold-standard FSC plots and local resolution heat maps for 80S rotated (top) and non-rotated (bottom) classes. (D) Custom masks were applied to the consensus reconstruction of WT RACK1 80S rotated state over the 60S (cyan), 40S body (pink), and 40S head (yellow). Signal subtraction was performed to delete signal outside of the mask, followed by local 3D refinement over the remaining signal. Local resolution heat maps shown for each component after local refinement. (E) Gold-standard FSC plots for the locally refined 60S, 40S body, and 40S head.

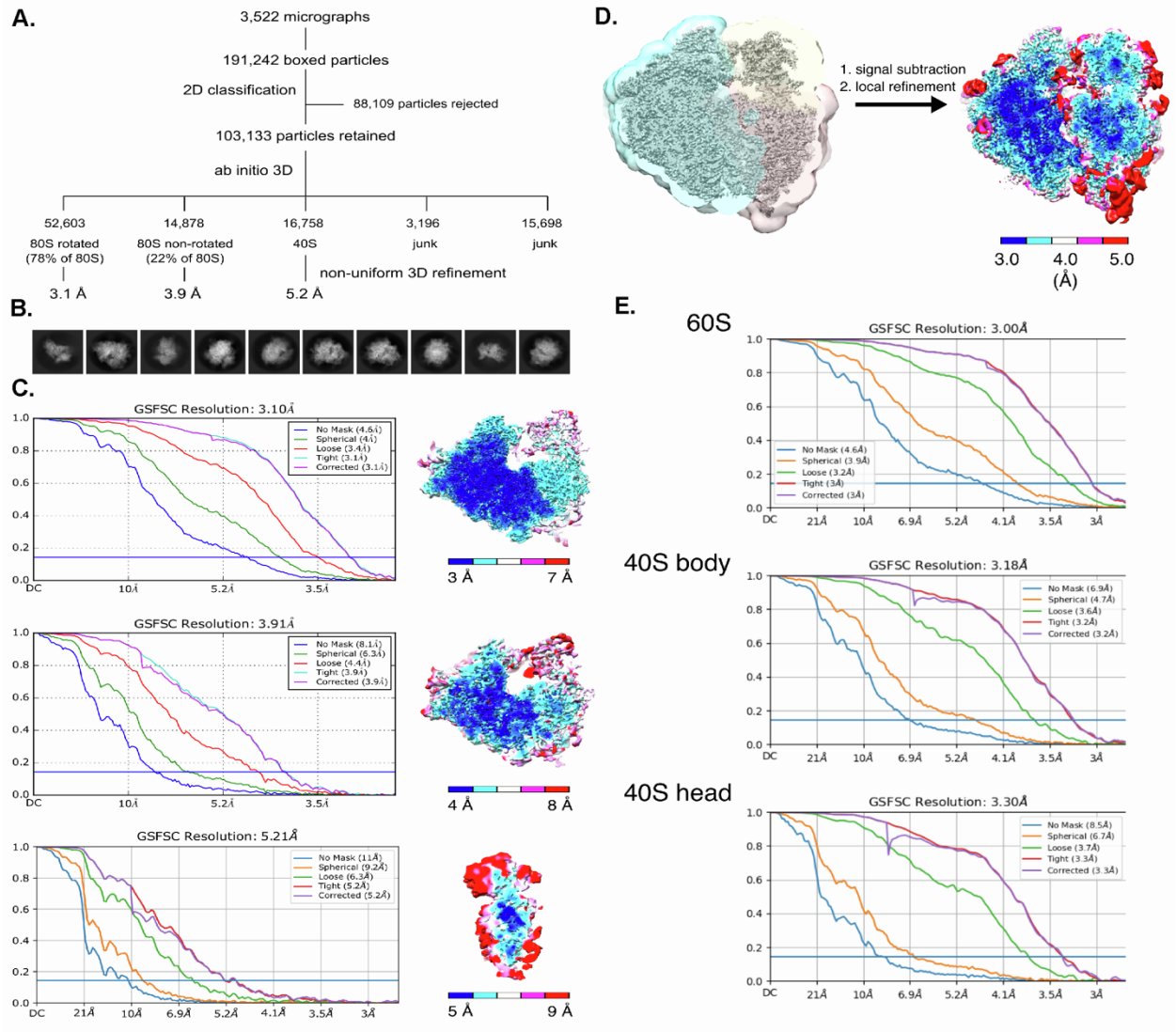

Figure S3: S^{278}E RACK1 cryo-EM data processing pipeline and local refinement of the 80S rotated state, related to Figure 1 and 5. (A) Data processing workflow and 3D classification scheme. (B) Representative reference-free 2D class averages of retained particles. (C) Gold-standard FSC plots and local resolution heat maps for 80S rotated (top), 80S non-rotated (middle), and 40S (bottom) classes. (D-E) The same workflow of masking and signal subtraction was applied for the S^{278}E RACK1 80S rotated dataset as described for WT RACK1 in Figure S2D-E.

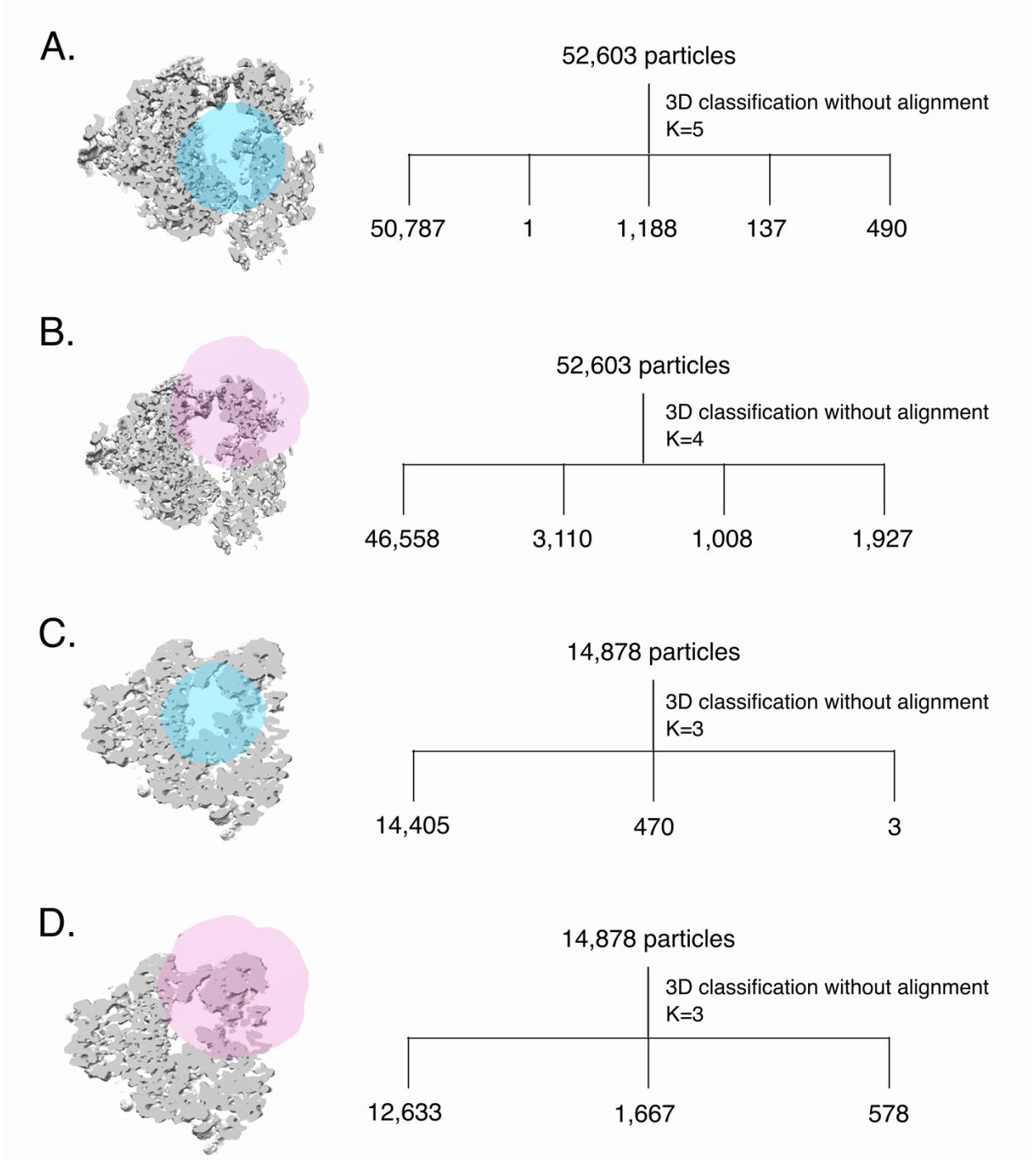

Figure S4: Focused 3D classification of S278E RACK1 80S rotated (A, B) and non-rotated (C, D) particles, related to Figure 1. Custom masks were applied to (A, C) the P-site tRNA binding site (blue) or (B, D) 40S head (pink) as the basis for focused 3D classification without particle realignment. Classification workflow indicates number of particles assigned to each class.

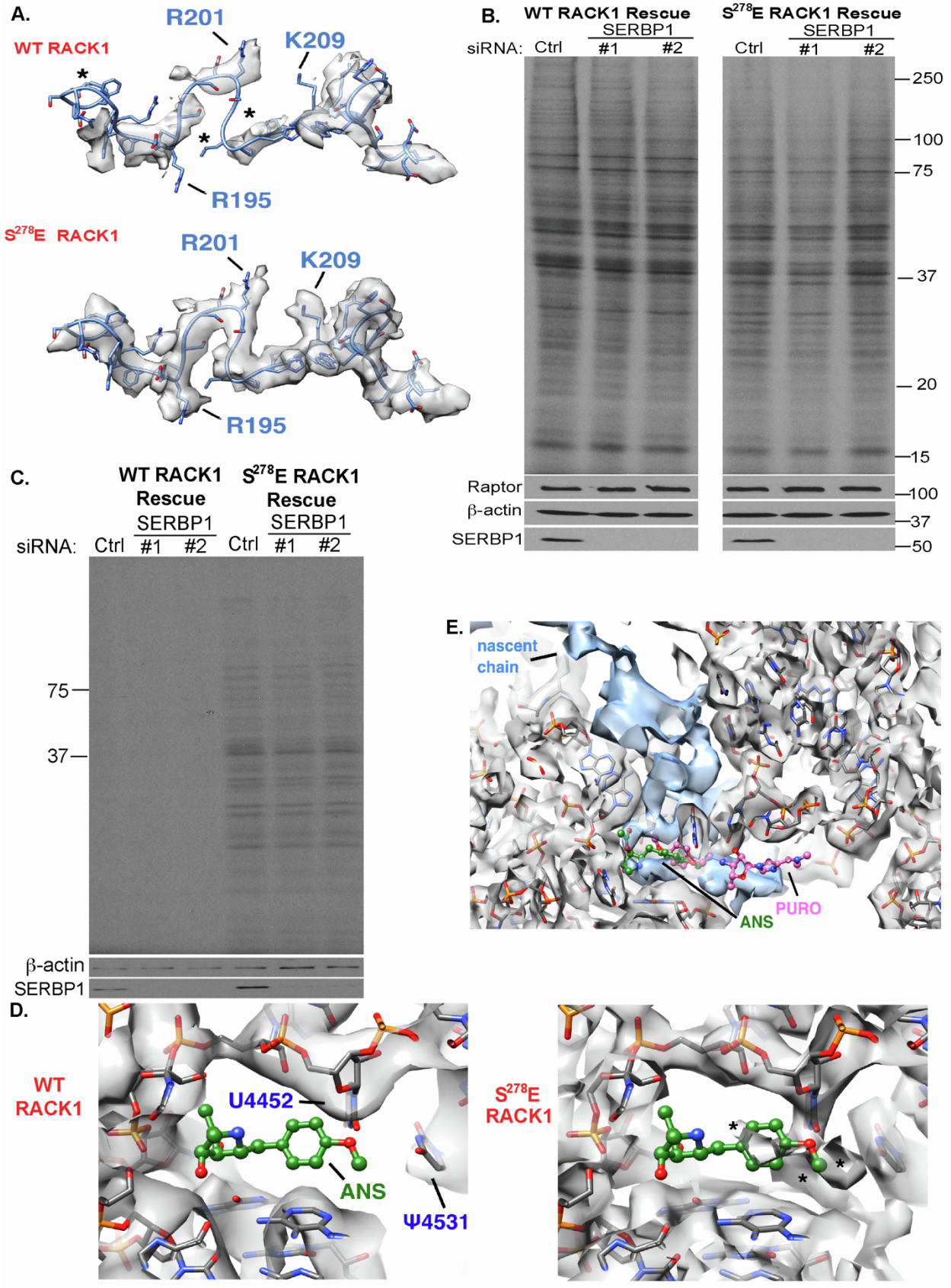

Figure S5: Characterization of SERBP1 and effects of S^{278}E RACK1 on anisomycin and puromycin binding

sites, related to Figure 1, 2 and 3. (A) View of SERBP1 model fitted in RACK1-WT (top) and $S^{278}E$ RACK1 (bottom) reconstructions indicate more ordered SERBP1 density in $S^{278}E$ RACK1. (B) siRNA-mediated depletion suggests that SERBP1 does not enhance translation in either WT or $S^{278}E$ RACK1-expressing cells. Cells were treated with control (ctrl) or either of two independent SERBP1 siRNAs prior to ^{35}S-Met/Cys pulse labeling. ^{35}S-Met/Cys labeling gel (top panel) and Western blot analysis (bottom panels) is shown. Representative of 3 independent biological replicates. (C) SERBP1 does not mediate resistance to cycloheximide in $S^{278}E$ RACK rescue cells. WT or $S^{278}E$ RACK1 cells were treated control (ctrl) or either of two independent SERBP1 siRNAs prior to treatment with cycloheximide and ^{35}S-Met/Cys pulse labeling. ^{35}S-Met/Cys labeling gels (top panel) and Western blot analysis (bottom panels) show that SERBP1 depletion does not impact the synthesis of proteins that are specifically sustained by $S^{278}E$ RACK1 in the presence of inhibitor. (D) View of anisomycin (ANS) binding site indicates unidentified clashing density in reconstruction of $S^{278}E$ RACK1 that is not observed in WT RACK1. ANS modeling based on PDB 4U3M (Garreau de Loubresse, 2014). (E) Zoomed out view of the $S^{278}E$ reconstruction showing putative nascent chain density (blue) and its proximity to anisomycin (green) and puromycin (pink) binding sites.

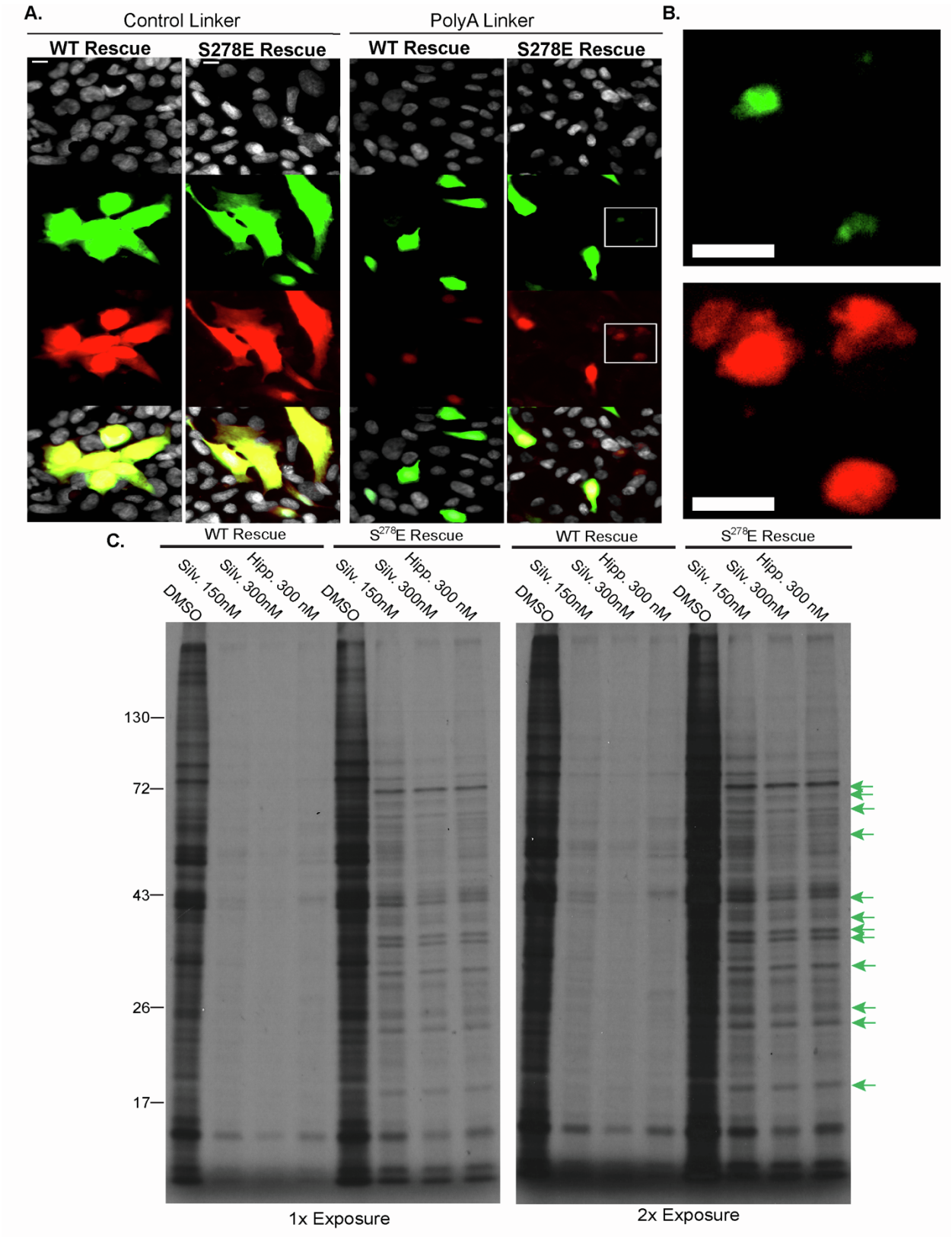

Figure S6: Effects of negative charge in the RACK1 loop on RQC reporter activity and eIF4A-dependent protein synthesis, related to Figure 3 and 4. (A-B) Representative images of GFP and RFP expression from control or polyA stall reporters analyzed in Figures 3 and 4. Note that in the control reporter, cells expressing either

WT or $S^{278}E$ RACK1 express equivalent levels of GFP and RFP. As expected, less RFP is produced relative to GFP from the polyA stall reporter in cells expressing WT RACK1. However, two cell populations are observed in cells expressing $S^{278}E$ RACK1; as shown in larger scale analysis in Figure 4A, in a smaller subset of cells less RFP is produced than GFP, as expected. But in a larger fraction of cells, very little GFP is made despite notable levels of RFP expression; zooms in B. highlight these cells. Bar = 10μm. (C) WT RACK1 or $S^{278}E$ RACK1 rescue cells were treated with the indicated concentrations of the eIF4A inhibitors, silvestrol (Silv.) or hippuristanol (Hipp.) prior to ^{35}S-methionine/cysteine pulse labeling. Complementing data in Figure 4C and 4D, this data provides a direct comparison of the effects of both inhibitors and enlarged autoradiograms make it easier to see resistant proteins in $S^{278}E$ RACK1 rescue cells (indicated with green arrows). Two exposures are provided side-by-side with the longer exposures illustrating the specificity of the resistant proteins in $S^{278}E$ RACK1 rescue cells.